



# HHS Public Access

Author manuscript

*Neurobiol Dis.* Author manuscript; available in PMC 2017 September 01.

Published in final edited form as:

*Neurobiol Dis.* 2016 September ; 93: 137–145. doi:10.1016/j.nbd.2016.05.003.

## Mouse model of rare *TOR1A* variant found in sporadic focal dystonia impairs domains affected in DYT1 dystonia patients and animal models

Srishti L. Bhagat<sup>1,2,\*</sup>, Sunny Qiu<sup>1,\*</sup>, Zachary F. Caffall<sup>1</sup>, Yehong Wan<sup>1</sup>, Yuanji Pan<sup>1</sup>, Ramona M. Rodriquez<sup>5</sup>, William C. Wetzel<sup>3,5</sup>, Alexandra Badea<sup>6</sup>, Ute Hochgeschwender<sup>1</sup>, and Nicole Calakos<sup>1,2,3</sup>

<sup>1</sup>Department of Neurology, Duke University Medical Center, Durham, NC 27710

<sup>2</sup>Department of Neurobiology, Duke University Medical Center, Durham, NC 27710

<sup>3</sup>Duke Institute of Brain Sciences

<sup>4</sup>Department of Biomedical Engineering, Duke University Medical Center, Durham, NC 27710

<sup>5</sup>Department of Psychiatry and Behavioral Sciences, Duke University Medical Center, Durham, NC 27710

<sup>6</sup>Department of Radiology, Duke University Medical Center, Durham, NC 27710

### Abstract

Rare *de novo* mutations in genes associated with inherited Mendelian disorders are potential contributors to sporadic disease. DYT1 dystonia is an autosomal dominant, early-onset, generalized dystonia associated with an in-frame, trinucleotide deletion (n. delGAG, p. E 302/303) in the *Tor1a* gene. Here we examine the significance of a rare missense variant in the *Tor1a* gene (c. 613T>A, p. F205I), previously identified in a patient with sporadic late-onset focal dystonia, by modeling it in mice. Homozygous F205I mice have motor impairment, reduced steady-state levels of TorsinA, altered corticostriatal synaptic plasticity, and prominent brain imaging abnormalities in areas associated with motor function. Thus, the F205I variant causes abnormalities in domains affected in people and/or mouse models with the DYT1 *Tor1a* mutation (E). Our findings establish the pathological significance of the F205I *Tor1a* variant and provide a model with both etiological and phenotypic relevance to further investigate dystonia mechanisms.

### Keywords

DYT1 dystonia; TorsinA; Behavior; Long-term depression; Diffusion tensor magnetic resonance imaging

---

Corresponding author: Nicole Calakos, nicole.calakos@duke.edu.

\*These authors contributed equally to this work

**Publisher's Disclaimer:** This is a PDF file of an unedited manuscript that has been accepted for publication. As a service to our customers we are providing this early version of the manuscript. The manuscript will undergo copyediting, typesetting, and review of the resulting proof before it is published in its final citable form. Please note that during the production process errors may be discovered which could affect the content, and all legal disclaimers that apply to the journal pertain.

## INTRODUCTION

Dystonia is a neurological movement disorder characterized by involuntary twisting movements and abnormal postures. Environmental, genetic and sporadic cases together make dystonia among the top 3 conditions evaluated in Movement Disorder specialty clinics (Nutt et al., 1988). Of the early-onset isolated dystonias, DYT1 dystonia is among the most common (Balint and Bhatia, 2015; Ozelius L, 1999 [Updated 2014]). DYT1 dystonia is an autosomal dominant disease with incomplete penetrance that is due to an in-frame trinucleotide deletion in the *Tor1a* gene resulting in the loss of a glutamic acid residue ( E) from the TorsinA protein (Bressman et al., 1989; Risch et al., 1990). It is an early-onset generalized dystonia, presenting in childhood and involving much of the body. In DYT1 dystonia, human neuroimaging abnormalities have been documented in several parts of the brain involved in motor function, including the cerebellum (Carbon et al., 2004b; Eidelberg et al., 1998), sensorimotor cortex (Carbon et al., 2004a; Carbon et al., 2008) and basal ganglia (Carbon et al., 2004b; Ghilardi et al., 2003; Tros t et al., 2002). Mouse DYT1 dystonia models share some of these neuroimaging motor circuit abnormalities (Grundmann et al., 2007; Ulug et al., 2011; Vo et al., 2014) and also have impaired synaptic plasticity in a brain region associated with dystonia expression, the striatum of the basal ganglia (Martella et al., 2014; Martella et al., 2009). Interestingly, phenotypic validity has not been as readily recapitulated in mouse heterozygous E knock-in models (Dang et al., 2005; Goodchild et al., 2005; Tanabe et al., 2012). Nonetheless, conditional genetic models that eliminate all wild-type protein (Liang et al., 2014; Pappas et al., 2015) or heavily over-express the protein (Grundmann et al., 2007) demonstrate proof-of-principle that TorsinA perturbations can impact motor behavior.

Rare variants in the *Tor1a* gene, as well as other genes associated with dystonia, have been reported in cases of sporadic dystonias (Calakos et al., 2010; Dobri i et al., 2015; Dufke et al., 2014; Groen et al., 2015; Groen et al., 2014; Hettich et al., 2014; Kock et al., 2006; Kumar et al., 2014; Lohmann et al., 2012; Nibbeling et al., 2015; Saunders-Pullman et al., 2014; Vemula et al., 2014; Vulinovic et al., 2014; Zech et al., 2014; Ziegen et al., 2014), suggesting this as one potential genetic contribution to disease. However, obtaining formal genetic support, as in association studies, is fundamentally challenged when rare genetic events occur in rare disorders. In this study, we tested the pathophysiological significance of a rare *Tor1a* variant by modeling it in mice. The missense variant, which results in the substitution of phenylalanine with isoleucine at the 205<sup>th</sup> residue (F205I), was originally identified as a heterozygous mutation in a sporadic, late-onset case of focal dystonia (Calakos et al., 2010). The variant lies in a highly evolutionarily conserved region of TorsinA suggesting functional importance of this region (Calakos et al., 2010). In prior work, we found that, similar to E TorsinA, F205I TorsinA protein mislocalizes and forms inclusions when over-expressed in cultured cells, though not to as severe a degree (Calakos et al., 2010). Nery and colleagues further showed that the F205I variant disrupts ER function (Hettich et al., 2014). These observations suggest that the mutation may be pathophysiologically significant. To determine the brain and behavioral significance of the F205I variant, we created a knock-in mouse model.

We found that homozygous F205I *Tor1a* mice have abnormalities in key domains affected in the DYT1 dystonia clinical disorder and/or mouse models: e.g. neonatal survival (Dang et al., 2005; Goodchild et al., 2005), cellular TorsinA levels (Goodchild et al., 2005; Hewett et al., 2006), synaptic plasticity (Martella et al., 2014; Martella et al., 2009), motor circuitry (Argyelan et al., 2009; Grundmann et al., 2007; Liang et al., 2014; Ulug et al., 2011; Vo et al., 2014) and movement (Tanabe et al., 2009). Notably, adult homozygous F205I *Tor1a* mice display context-dependent motor impairments in multiple behavioral tasks. Thus, the presence of both brain and behavioral abnormalities in F205I *Tor1a* mutant mice affords a valuable new model to advance dystonia research.

## METHODS

### Generation of knock-in mice

Using homologous recombination, exon 3 of the murine *Tor1a* gene was altered to encode isoleucine at amino acid position 205 as well as a silent mutation to introduce a restriction site to facilitate genotyping recombinant mice. A targeting construct was generated encompassing 3 homology regions of the mouse TorsinA genomic sequence: the Short Homology Arm (SA) encoding ~1Kbp upstream of the region for mutation, the Middle Homology Arm (MA) containing the region for mutation (exons 3 and 4), and the Long Homology Arm (LA) encoding ~10Kbp downstream of the region for mutation. Each homology arm was retrieved using recombination from Bacterial Artificial Chromosomes (BACs), acquired from Source BioScience (bMQ225J10 & bMQ440P11; Santa Fe Springs, CA), containing the genomic sequence for the *Tor1a* gene. The SA was cloned into a plasmid (pFLN-TK) upstream of a LoxP site and a Neomycin (Neo) cassette flanked by Flippase Recognition Target sequences (Frt). The MA was mutated to incorporate the F205I mutation and an adjacent translationally silent mutation to generate a novel *SspI* restriction site by Site-Directed Mutagenesis using Stratagene's QuikChange Multi Site-Directed Mutagenesis Kit (Agilent, #210516). The mutated MA was then sub-cloned into the pFLN-TK plasmid downstream of the SA-Neomycin Cassette. The LA was subsequently sub-cloned into the same plasmid after the second LoxP site, thus creating the targeting construct. The linearized targeting construct was electroporated into 129sv ES cells. Colonies were screened for homologously recombined clones by PCR and confirmed with Southern Blot. The ES cells were injected into mouse blastocysts and implanted in pseudo pregnant females. Chimeric mice were bred to C57BL/6 to produce agouti founders for the line used in this study, which was maintained as a hybrid strain. Genotyping was performed using PCR oligonucleotide primers. Primers used in PCR are as follows (5' to 3'): sense TCCTTCAGGACCAGTTACAG and antisense TTCCTCCACAAGGAATGTAG. PCR was followed by digestion with the *SspI* restriction enzyme (New England Biolabs, Massachusetts).

### Mouse experimental subjects

All animal procedures were performed in accordance with protocols approved by the Institutional Animal Care and Use Committee of Duke University. Experiments were performed on both male and female mice that were either wildtype (WT), heterozygous (HT) or homozygous (HOMO) for the F205I mutation maintained on a hybrid strain

background of 129/Sv and C57BL/6. To control for strain effects, littermate controls produced by heterozygous crosses were used, and all results were derived from experimental subjects from multiple distinct breeding pairs. For electrophysiology experiments, mice were crossed with the *Drd2*-EGFP line (Gong et al., 2003) or the *Drd1a*-tdTomato line (Shuen et al., 2008) to distinguish the two major subtypes of medium spiny neurons. Genotypes for all experimental subjects were re-confirmed *post mortem*.

### Human subjects and fibroblast cell lines

The human subjects research protocol for tissue collection to establish the F205I dermal fibroblast culture was approved by the Duke University Institutional Review Board (IRB) and the subject gave written informed consent and provisions to protect patient privacy. The subject was recruited at the Parkinson and Movement Disorders Center at Duke University Medical Center, Durham, North Carolina, USA. Control (Line IDs: GM00023 & GM02037) and E (Line IDs: GM02306 and GM03208) human patient dermal fibroblast lines were acquired through the NINDS Repository at the Coriell Institute for Medical Research, in compliance with the Coriell Institute of Medical Research's IRB, which includes informed consent and privacy protections.

### Western immunoblotting and immunohistochemical techniques

Forebrain and midbrain of 2–4 week old wildtype, F205I heterozygous, F205I homozygous, and E heterozygous mice were dissected and chilled in phosphate buffered saline. Tissue was then homogenized on ice in lysis buffer (50mM Tris-HCl, 100mM NaCl, 2% SDS, pH 7.4, with cOmplete Mini EDTA-free protease inhibitor (Roche #04693116001), extracted for 1–2 hours at 4°C on a rotator, and centrifuged at 16000×g for 30 minutes at 4°C. Protein concentration of supernatant was measured using the Pierce bicinchoninic acid (BCA) assay (Thermo Fisher Scientific #23225). Protein was resolved on a 4–20% Mini-PROTEAN TGX polyacrylamide gel (Bio-Rad), transferred to a nitrocellulose membrane, blocked in Tris-buffered saline with Tween (TBS-T) + 5% non-fat dry milk and probed with anti-TorsinA antibody (Abcam, ab34540). To control for gel loading, blots were additionally probed with anti-β-actin (Chemicon, MAB1501).

Human fibroblast cells from primary cultures were harvested in radioimmunoprecipitation assay (RIPA) buffer (Chung et al., 2000) supplemented with phosphatase inhibitor cocktail (Sigma #P5726) and cOmplete Mini EDTA-free protease inhibitor (Roche #04693116001). Total protein concentrations were assessed by BCA assay (Thermo Fisher Scientific #23225). Proteins were resolved on 4–15% TGX gels (Bio-Rad #5671085), transferred to nitrocellulose membrane, blocked in TBS-T + 5% non-fat dry milk, and probed as indicated.

### Striatal electrophysiology

Slices were prepared from P14–21 mice as described previously (Wan et al., 2011). In brief, mice were anesthetized and transcardially perfused with ice-cold carboxygenated high-sucrose artificial cerebrospinal fluid (aCSF). After a one hour recovery period in carboxygenated standard aCSF at room temperature, recordings were made at 32°C, in the presence of 50 μM picrotoxin, from EGFP-positive cells or tdTomato-negative cells (striatopallidal medium spiny neurons). High-sucrose aCSF contained (in mM): 194 sucrose,

30 NaCl, 4.5 KCl, 1.2 NaH<sub>2</sub>PO<sub>4</sub>, 0.2 CaCl<sub>2</sub>, 2 MgCl<sub>2</sub>, 26 NaHCO<sub>3</sub>, and 10 D-(+)-glucose and standard aCSF contained (in mM): 124 NaCl, 2.5 KCl, 1.2 NaH<sub>2</sub>PO<sub>4</sub>, 2 CaCl<sub>2</sub>, 1 MgCl<sub>2</sub>, 26 NaHCO<sub>3</sub>, and 10 D-(+)-glucose. Stimulation was delivered using a twisted bipolar electrode made from tungsten wire (A-M Systems Inc., Cat.# 796500), with stimulation intensity set to evoke an approximately half-maximal response. Responses were monitored with a 30 s inter-stimulation-interval. Long-term depression (LTD) was induced by standard protocol (Chen et al., 2011; Choi and Lovinger, 1997): four 100 Hz trains of 1 s duration (10 s inter-train interval) were paired with depolarization to 0 mV, and stimulus intensity during high-frequency stimulation (HFS) was increased to the minimum intensity that evoked the maximal evoked response.

### Behavioral tests

**Novel open field test**—Adult mice, aged 2–3 months, were placed in unfamiliar 20cm × 20cm × 20cm modified open field arenas with lids and activity was monitored for 30 minutes with infrared sensors (Omnitech Electronics).

**Homecage open field test**—Adult mice, aged 7–8 months, were placed in 20cm × 20cm × 20cm modified open field arenas with lids, along with bedding from their native cage and food and water, and activity was monitored for 72 hours with infrared sensors (Omnitech Electronics). Because there were no significant differences between the 3 individual days of testing, mean activity over a 24 hour time period was calculated by taking the average over three days for each time period.

**Treadmill test**—Adult mice, aged 3–12 months, were placed in a 33cm × 5cm × 17cm motorized treadmill chamber (TreadScan, CleverSys). The initial speed of the treadmill was set at 15 cm/s, and lowered incrementally to find the maximum speed at which a mouse could maintain active ambulation for at least 2 min.

**Accelerating rotarod**—Adult mice, aged 2–5 months, were placed on a five station rotarod (Med Associates, Inc.). Rotarod testing was performed using a steady acceleration protocol of 4 to 40 revolutions per minute (RPM) over 5 minutes, followed by a constant 40 RPM speed for 5 min. The total time mice were able to actively run on the rotarod was recorded. Trial completion was marked by any of the following (1) running for a total of 10 min (2) falling from the rotarod (3) clinging to the rotarod without taking any steps for 2 complete revolutions. Testing consisted of three trials/day for three consecutive days, with inter-trial intervals of 15 minutes for each mouse. An animal's performance was calculated by taking the average of the three daily trials.

**Wire hang**—As previously described (Niimi et al., 2009), adult mice, aged 2–3 months, were placed on a wire coat hanger with only front paws grabbing onto the horizontal bar. Mice were scored on a 0–5 scale as follows: 0 – immediately fell, 1 - hung onto the bar with both forepaws, 2 - hung onto the bar and made attempts to climb fully onto the bar, 3 - hung onto the bar with both forepaws and at least one hindpaw, 4 - hung onto the bar with all four paws with tail wrapped around the bar, 5 - traversed the bar and escaped. Testing consisted of 3 trials, with inter-trial intervals of 15 minutes for each mouse.

**Grip strength**—Adult mice, aged 2–3 months, were tested as previously described (Allen et al., 2009). Mice were held by the tail and lowered onto the metal grid of a grip strength meter (Harvard Apparatus) so their front paws gripped the grid. They were pulled backwards horizontally, and the peak force applied just before losing grip was recorded in grams of force generated. Mice were also held by the tail and lowered onto the metal grid so both front and rear paws gripped the grid. They were again pulled backwards, and the peak force applied just before losing grip was recorded in grams of force generated. Testing consisted of three trials for both front paws and all paws. Average grip strength of front and all paws was calculated over three trials.

### Magnetic Resonance Imaging (MRI)

Six homozygous mice and six littermate wildtype controls, sex matched, were imaged for volumetric analysis and fractional anisotropy (FA). Mouse brain specimens were prepared as previously described (Badea et al., 2010; Johnson et al., 2002), with slight modification. Animals were anesthetized and perfused with a solution of 0.9% phosphate buffered saline (PBS), at a rate of 5 ml/minute, for 5 minutes. Fixation proceeded with a 10% solution of Neutral Buffered Formalin (NBF) containing 10% (50 mM) Gadoteridol (ProHance, Bracco Diagnostics, Monroe Township, NJ), at a rate of 5 ml/minute for 5 minutes. Mouse heads were stored in 10% NBF for 24 h, then transferred to a 0.1 M solution of Phosphate Buffered Saline containing 1% (5 mM) Gadoteridol at 4 °C for 7–10 days to rehydrate the tissue. Extraneous tissue around the cranium was removed prior to imaging, and specimens were placed in MRI-compatible tubes, immersed in perfluoropolyether (Galden Pro, Solvay, NJ), for susceptibility matching and to prevent dehydration. Specimens were scanned within the cranium, to avoid tissue damage and possible distortions.

To measure the morphometric and diffusion properties of the brain tissue, MR imaging was done at 9.4 T, 8.9 cm vertical bore Oxford magnet, with shielded coils providing gradients of up to 2000 mT/m (Resonance Research, Inc. Billerica, MA), controlled by a Agilent Direct Drive Console (Agilent Technologies, Santa Clara, CA). We used a diffusion tensor imaging protocol to measure the diffusion properties of the tissue. This sequence used 6 diffusion directions, and TE=12ms, TR=100ms,  $b \approx 1595 \text{ s/mm}^2$ ; diffusion pulse width = 1.3 ms, separation = 5ms, duration 4.04 ms, amplitude 90.94 G/cm). Images were acquired over  $22 \times 11 \times 11 \text{ mm}$  field of view, with a matrix of  $512 \times 256 \times 256$ , and reconstructed at  $43 \mu\text{m}$  isotropic resolution. The scan durations were ~12 hours.

For image analysis, we used a segmentation pipeline (Badea et al., 2012) and a second generation reference mouse brain atlas, available from <http://www.civm.duhs.duke.edu/waxholmspace2/> and based on (Johnson et al., 2010), to provide priors for automated segmentation of 101 regions. MATLAB (MathWorks, Natick, MA) was used to compute statistics from a two-tailed t-test for MR-based regional measurements for volume, and diffusion tensor parameters. We note that one of the F205I homozygotes had to be excluded from FA analysis due to poor technical quality of scan, i.e. lower signal to noise ratio (SNR) than the other brains. Advanced Normalization Tools (ANTs) (Avants et al., 2008; Avants et al., 2014) was used for image registration of the FA images derived from diffusion tensor imaging (DTI), to generate a minimum deformation template (MDT), which was in turn

registered to the atlas. The resulting transforms were used to map the reference atlas labels onto individual brains, and to map all DTI parametric images into the space defined by MDT. SurfStat (Chung et al., 2010) was used for statistical parametric mapping, and Avizo (VSG Inc., Burlington, MA, USA) for visualization. The significance level was set to  $p < 0.05$  for uncorrected statistics, and false discovery rate (FDR) to 0.05 for corrected statistics.

### Statistical analysis

Statistical analysis was performed using GraphPad Prism 6 (GraphPad Software Inc.) and JMP 11 Pro (SAS Institute Inc.). Text and figure legends specify the statistics used for each dataset. Outliers greater than two standard deviations above the mean for each genotype were removed (2 HT from homepage OFT, 1 HT from novel OFT, 1 WT from grip strength). To compare across multiple genotypes, one-way analysis of variance (ANOVA) was used, with Holm-Sidak or Dunnett's *post hoc* multiple comparisons tests, as appropriate. For experiments with an additional variable of time, two-way ANOVA was performed, with Holm-Sidak *post hoc* multiple comparisons test. For non-parametric data, Chi-square test and Fisher's exact test were used as described in the text and figure legends. Significance was set to  $\alpha = 0.05$  for corrected statistics. Data are presented as mean  $\pm$  SEM for all numeric data with continuous distributions.

## RESULTS

### **F205I homozygotes have reduced perinatal mortality compared to E homozygotes, consistent with a weaker allelic effect**

F205I knock-in mice were generated using standard homologous recombination techniques. Genotyping confirmed that mice were born in Mendelian ratios. At birth, mice could not be distinguished by appearance or weight. However, by the second week of life, homozygotes developed marked weight loss and impaired motor coordination (Figure 1A, Supplemental Figure 1, Supplemental Videos). Approximately half of the homozygous mice died by the third postnatal week (Figure 1B). However, those that survived show near normal adult weights (Figure 1C) and normal lifespan. Since homozygous E *Tor1a* mutation causes 100% mortality of mice within 48 hours after birth (Goodchild et al., 2005), these data indicate that the F205I mutation of *Tor1a* is less severe than the E allele.

### **F205I variant reduces steady-state TorsinA levels in patient-derived fibroblasts and knock-in mouse brain**

In both patient-derived cell lines (Hewett et al., 2006) and knock-in mouse models (Goodchild et al., 2005), the DYT1 E mutation has been associated with a reduction in steady-state TorsinA levels. Here we examined whether the F205I mutation influenced TorsinA protein levels. Although TorsinA dysfunction in the brain presumably underlies dystonia, TorsinA can also be examined in peripheral tissues since it is expressed throughout the body (Ozelius et al., 1997). Therefore, we first examined TorsinA levels in fibroblasts derived from the index patient. F205I human fibroblasts showed reduced TorsinA levels in comparison to similarly processed lines from healthy controls (Figures 2A and B). Next we examined brain tissue from F205I knockin mice. We found that, as has been described in E

knock-in mice (Goodchild et al., 2005), the F205I mutation caused a gene dose-dependent effect of reducing TorsinA levels (Figures 2A and C). These findings demonstrate a shared cellular phenotype between the E mutation and the F205I variant in both patient-derived tissue and the knock-in mouse model.

### **Homozygous F205I mice display numerous motor coordination abnormalities in novel environments**

As has been reported in mouse models of DYT1 dystonia (Goodchild et al., 2005; Tanabe et al., 2012), mice heterozygous for the F205I *Tor1a* allele had no appreciable motor phenotype. However, in F205I mice bearing two mutant alleles, motor abnormalities were readily distinguishable. Homozygous F205I mice were the most phenotypically affected in the P14–P21 perinatal period. Mice displayed freezing, tremor and abnormal ambulation (Supplemental Video 1–4). These symptoms were exacerbated by mild stressors such as handling the mice or placing them in a novel environment. As an example, supplemental feeding by oral gavage was not tolerated and resulted in death of homozygous mice, whereas wildtype littermates tolerated this procedure without incident.

Interestingly, by adulthood, surviving homozygous F205I mice were not readily distinguished from wildtype littermates on casual observation. In support of this, adult F205I homozygotes had normal activity levels in their native home cage environment (Figure 3A) and did not display gross abnormalities in SHIRPA screening of motor, sensory, spinocerebellar, and autonomic functions (Supplemental Table 1). However, we observed that when mice were placed into a novel, but otherwise standard open field arena, adult F205I homozygotes had significantly lower activity levels than their wildtype counterparts (Figure 3B). These differences lessened with time in the new environment, suggesting a role for environmental novelty and/or handling stress. This time course (i.e. approximately after initial 30 minutes) also corresponds to the time course during which normal mice adapt to a new environment as indicated by locomotor exploration reaching a plateau (Jew et al., 2013).

To further test for the possibility of novelty/stress-induced motor impairment, we performed several additional more challenging motor tasks. In the novel environment of a motorized treadmill, we found that a higher proportion of mutant mice were unable to perform the task at treadmill speeds easily tolerated by wildtype littermates (Figure 3C). At times, poor performance was accompanied by dystonic-like abnormal tail postures, trunk hunching and slower uncoordinated hindlimb movements (Supplemental Video 5). In the accelerating rotarod task, F205I homozygotes again performed worse than littermate wildtype and heterozygous mice (Figure 3D). However, this was only noted on the initial day of training. Consistent with an interaction between novelty and test performance, upon repeated daily testing, F205I homozygotes improved their rotarod performance, achieving performance levels approximating that of their wildtype littermates. These data demonstrate that F205I homozygotes have intact motor learning and intact ability to ambulate (Figure 3D). Additionally, it is noteworthy that at 40 RPM on the accelerating rotarod, mice would need to run at 6.66 cm/s, so the minimum treadmill speed of 3 cm/s was well within the physical abilities of adult F205I homozygotes. Finally, in a wire hang task, which assesses

coordination, balance, and motor strength (Kawashita et al., 2014), mice were scored for their ability to climb a coat hanger, using a nonparametric rating system (Niimi et al., 2009). Again, F205I homozygotes performed significantly more poorly than wildtype littermates (Figure 3E). To ensure that score differences were not due to differences in strength, mice were also tested for grip strength. No differences in grip strength were observed (Figure 3F), indicating that F205I homozygotes have difficulties in coordinated movement not explained by primary defects in strength or body habitus. Thus, in multiple behavioral tests involving novel, challenging tasks, the F205I genotype is associated with poorer motor performance.

### **Impaired long-term depression of corticostriatal synapses in homozygous F205I mice**

Abnormalities in corticostriatal synaptic plasticity have been described in several mouse models for DYT1 dystonia (Dang et al., 2012; Martella et al., 2014; Martella et al., 2009). Specifically, impairment of corticostriatal long-term depression (LTD) in striatal projection neurons has been reported (Dang et al., 2012; Martella et al., 2014; Martella et al., 2009). To evaluate the integrity of this form of plasticity in the F205I model, we performed whole-cell, voltage-clamp recordings of evoked excitatory post-synaptic currents (ePSCs) in striatopallidal projection neurons and induced LTD as in (Chen et al., 2011; Choi and Lovinger, 1997). We found that, in comparison to littermate controls, homozygous F205I mice and E heterozygotes showed significantly reduced LTD (Figure 4). These results indicate that the E and F205I *Tor1a* mutations also share impairments in corticostriatal synaptic plasticity.

### **MR imaging of F205I homozygotes shows voxel-based morphometry and DTI abnormalities**

Both humans and mouse models bearing the E mutation of *Tor1a* have diffusion tensor magnetic resonance imaging (DT MRI) abnormalities (Carbon and Eidelberg, 2009; Carbon et al., 2004a; Grundmann et al., 2007; Vo et al., 2013b; Vo et al., 2014). We therefore performed DT MRI, using 9.4 T magnetic field strength, to evaluate morphometric and diffusion tensor parameter related phenotypes throughout the brains of F205I homozygous mice and littermate controls.

Voxel-wise comparisons of FA differences in DTI did not survive false discovery rate (FDR) correction at 5%. At the level of uncorrected statistics ( $p < 0.05$ ), FA was increased in areas of the corpus callosum, pontine structures, inferior colliculus, hippocampus, and orbital cortex (Figure 5A). FA was reduced in areas of the corpus callosum in the areas below the cingulate cortex (A29), M1/M2, parietal association cortex and S1, the brachium of the superior colliculus, deep cerebellar white matter, inferior cerebellar peduncle, and medial amygdaloid nucleus (Figure 5A). Some of these clusters were not symmetric in the same coronal slices; however, a contralateral cluster was found in neighboring slices. Notably, FA differences in cerebellar, pontine, and callosal structures have been previously associated with DYT1 dystonia (Carbon et al., 2008; Grundmann et al., 2007; Ulug et al., 2011; Vo et al., 2014).

We also performed both voxel-based and regional atlas-based morphometry comparisons to assess volume changes throughout the brain. Interestingly, in the F205I model, volume

changes were significantly more apparent than FA changes. Overall, the brain volume in homozygous F205I mice was 10% smaller ( $402 \pm 15 \text{ mm}^3$ ) relative to littermate controls ( $449 \pm 17 \text{ mm}^3$ ,  $p = 6.89 \times 10^{-4}$ ). However, body weight was not significantly different (WT  $26.32 \pm 1.42 \text{ g}$ , F205I HOMO  $25.46 \pm 2.45 \text{ g}$ ;  $p = 0.76$ , t-test). After correcting for global brain size differences, we proceeded to examine regional and voxel-wise volume changes. In voxel-wise comparisons (FDR corrected at 5%), we identified specific areas of significant differences in superior colliculus, red nucleus, lateral cerebellum, decussation of the superior cerebellar peduncles, pons, and a number of nuclei in the pontomedullary junction (e.g. reticular, raphe, medullary reticular and gigantocellular) (Figure 5B). Overall, these results reveal a predominance of hindbrain involvement.

Volumetric analysis using an atlas-based segmentation protocol with imaging priors and 101 manually delineated labels also revealed a number of gray and white matter regions with significant volume changes in homozygous F250I mice (Supplemental Table 2). The most significant differences surviving FDR correction at  $p < 0.05$  were reductions in volume for gray matter structures like the deep mesencephalic (13.5% reduction,  $p = 0.0008$ ), pontine (11% reduction,  $p = 0.009$ ), and raphe (8.73%,  $p = 0.032$ ) nuclei, as well as in white matter tracts including the superior (8.94%,  $p = 0.025$ ), and middle cerebellar peduncles (10.1%,  $p = 0.045$ ).

Finally, we applied the atlas-based segmentation protocol to analyze the FA signal data. We expected this analysis to be less sensitive because the pre-defined atlas regions commonly included significant areas of gray matter which could weaken signals deriving solely from white matter. We did not observe any significant differences in regional FA values that surpassed FDR correction at 5% level. Uncorrected statistics identified a significant difference in the inferior cerebellar peduncle (8.5% reduction,  $P = 0.006$ ) and modest trends ( $p < 0.1$ ) were present in the brachium of the superior colliculus (5% reduction,  $P = 0.07$ ), the posterior commissure (8% reduction,  $P = 0.08$ ) and the gigantocellular reticular nucleus (9% increase,  $P = 0.09$ ) (Supplemental Figure 2).

In summary, volume loss detected by MRI reflects a preponderance for the hindbrain regions, like brainstem, and cerebellum as reported in humans (Zweig et al., 1988) and rodent models (Oleas et al., 2014; Song et al., 2014) of primary dystonia.

## DISCUSSION

Rare variants in known disease-related genes are potential contributors to sporadic disease. Here, we show that the F205I rare variant of *Tor1a* causes brain and motor phenotypes when modeled in mice. Mouse models of DYT1 (E) dystonia have been inconsistent in producing a robust phenotype (Dang et al., 2005; Tanabe et al., 2012). Here, we report that mice homozygous for the F205I variant show motor deficits in a number of behavioral assays. Motor coordination deficits were seen in open field, accelerating rotarod, wire hang, and treadmill tests. In addition, MRI findings showed volumetric differences and DTI trends in a number of motor circuit regions for which abnormalities have been previously reported in DYT1 dystonia patients and mouse models. Thus, the F205I mouse model may provide a useful tool for studying disease pathology and testing novel treatments.

Several aspects of both the clinical and mouse model phenotypes suggest that the F205I mutation has a weaker allelic effect than the E mutation. The F205I mutation was observed in a patient with adult-onset, focal dystonia, a clinical syndrome that is less severe than the early onset, generalized dystonia caused by the E mutation (Calakos et al., 2010). In cell line studies, overexpression of the E or F205I mutations each caused a statistically significant increase in aberrant inclusions over similarly expressed wildtype TorsinA protein (Calakos et al., 2010). However, the degree of inclusions caused by the F205I mutation was statistically significantly less than that caused by the E mutation (Calakos et al., 2010). In the present study, when the F205I mutation is modeled in mice, we find that F205I homozygotes have less perinatal mortality than E homozygous mice (Dang et al., 2005; Goodchild et al., 2005). Interestingly, perinatal mortality of F205I homozygotes peaks in the second postnatal week. This period coincides with the peak of TorsinA expression (Vasudevan et al., 2006) and is similar to the peak mortality period of a phenotypic conditional CNS deletion model (Liang et al., 2014). Although heterozygous E mice have been inconsistent in producing a reliable motor phenotype, recently, conditional genetic models that eliminate all wildtype TorsinA in a subset of brain neurons have proven sufficient to cause motor phenotypes and neural degeneration (Liang et al., 2014; Pappas et al., 2015). The motor impairments observed in F250I homozygotes and in conditional genetic models (Liang et al., 2014; Pappas et al., 2015) indicate that mice can develop motor impairments due to TorsinA dysfunction, but further suggest that there may be a threshold of TorsinA dysfunction necessary to cause symptoms in mice.

As indicated by the reduced penetrance of DYT1 dystonia in humans, there are likely multiple genetic and/or environmental factors necessary for symptom expression. Although here we report a robust phenotype in a hybrid strain background, we also found that the phenotype was affected by mouse strain (data not shown). Similar influences have been reported for the E knock-in model (Tanabe et al., 2012). Of note, opposite to that study which indicates that the C57Bl/6 strain worsened the E phenotype, we found that the F205I phenotypes were weakened by C57Bl/6 backcrossing.

A notable feature of the behavioral phenotype of the F205I homozygous mice is that motor performance is impaired in testing situations which are novel and/or challenging. For example, F205I homozygotes have less activity than wildtype mice in the novel open field test, but do not behave differently in their home cage, either to casual observation or locomotor measures. F205I homozygotes also perform worse than wildtypes on the first day of accelerating rotarod, but show normal performance and learning on subsequent test days. In clinical populations, stress can be a contributor to dystonic symptoms (Dauer et al., 1998; de Carvalho Aguiar et al., 2004). Additionally, acute stress is necessary to elicit behavioral deficits in an animal model of DYT12 dystonia (DeAndrade et al., 2011), suggesting that stress may precipitate motor symptoms in susceptible mice. In F205I homozygotes, our findings suggest that stress due to novel situations is necessary for motor deficits, although the mechanism by which this occurs is presently unclear.

Motor circuit abnormalities were also apparent in electrophysiological and MRI studies of homozygous F205I mice. F205I homozygotes show impairments in corticostriatal LTD, similar to well-described LTD reductions reported in E knock-in heterozygotes (Martella et

al., 2014; Martella et al., 2009) and reproduced here (Figure 4B). In human neuroimaging studies, the E dystonia mutation has been associated with changes in cerebello-thalamo-cortical sensorimotor pathways (Neychev et al., 2011; Vo et al., 2013a). The E knock-in mouse model reproduces several of the human neuroimaging abnormalities. In MR imaging of F205I homozygous mice, we found that a number of the same brain regions were affected, though more so in volumetric than FA analyses. To our knowledge, this is the first voxel-based morphometry analysis of effects of *Tor1a* mutation in mice. Like E mice and humans, homozygous F205I mice showed subcortical white matter, pontine and cerebellar involvement (Argyelan et al., 2009; Carbon et al., 2004a; Carbon et al., 2008; Grundmann et al., 2007; Ulug et al., 2011; Vo et al., 2014). While the superior and middle cerebellar peduncles were reduced in volume, the FA was reduced for the inferior cerebellar peduncle. The red nucleus was also notably affected in F205I homozygotes. Interestingly, this region was also affected in histological analysis of a phenotypic conditional genetic *Tor1a* model (Liang et al., 2014). Overall, these MRI findings reveal that the F205I model shares susceptibility in a number of brain regions affected in DYT1 dystonia.

These findings also suggest that alterations in overall motor circuitry, as opposed to a single brain region, may drive pathology. This result is consistent with idea that multiple components of motor circuitry may be important for the expression of dystonia (Calderon et al., 2011; Tanabe et al., 2009). In particular, we find that areas besides the basal ganglia are affected in homozygous F205I mice, including the red nucleus, reticular formation and cerebellum. Finally, because of the higher spatial resolution enabled by imaging fixed mouse brain relative to standard human MRI technology, our findings provide an example of how rodent models can help identify the involvement of specific nuclei and tracts, particularly in brainstem, to help better understand their role in dystonia.

## CONCLUSIONS

Here we present a novel phenotypic mouse model based on a rare *Tor1a* missense variant identified in a case of sporadic focal dystonia. We find that because the F205I mutation has a weaker allelic effect than the E allele, homozygous mice survive, providing an opportunity to examine a behaviorally symptomatic mouse model. The homozygous F205I mouse model shares a number of features previously associated with DYT1 dystonia studies in humans and mouse models, including reduced steady-state TorsinA levels, impaired corticostriatal synaptic plasticity, and motor circuit brain imaging abnormalities. These findings support a pathogenic role for the rare variant F205I *Tor1a* in dystonia and provide a novel mouse model with aspects of both construct and face validity to facilitate future investigations into causes and treatments for dystonia.

## Supplementary Material

Refer to Web version on PubMed Central for supplementary material.

## Acknowledgments

The authors gratefully acknowledge financial support for this work by research grants from the Bachmann-Strauss Dystonia and Parkinson Foundation and Jake's Ride for Dystonia Research to N.C., the National Institutes of

Health (NS072707-01A1 to N.C.; K01AG041211-03 to A.B.; T32-746-GM007171 Medical Scientist Training Program to S.B.), Duke University (Duke Institute for Brain Sciences Incubator Award and Duke Core Facility Award to N.C.; Holland-Trice Fellowship to S.B.; Duke University Deans' Summer Research Fellowship and Duke University Undergraduate Research Assistantship to S.Q.), and the American Foundation for Pharmaceutical Education (Wakeman Fellowship to S.B.). We acknowledge use of the Duke University Center for *In Vivo* Microscopy (supported by NIH P41 EB 015897 and 1S10OD010683-01).

The authors are grateful to the staff of the Neurobehavioral Core Facility (in particular, Chris Means and Theo Rhodes) for assistance with behavioral testing, Nicholas Katsanis and Edwin Oh for assistance establishing primary fibroblast cultures, Christina Christensen and Raehum Paik for technical assistance, and most importantly, our deepest gratitude for the participation of our patients in this research.

## REFERENCES

- Allen KD, et al. Decreased Physical Function and Increased Pain Sensitivity in Mice Deficient for Type IX Collagen. *Arthritis and rheumatism*. 2009; 60:2684–2693. [PubMed: 19714629]
- Argyelan M, et al. Cerebello-Thalamo-Cortical Connectivity Regulates Penetrance in Dystonia. *The Journal of Neuroscience*. 2009; 29:9740–9747. [PubMed: 19657027]
- Avants BB, et al. Symmetric diffeomorphic image registration with cross-correlation: evaluating automated labeling of elderly and neurodegenerative brain. *Med Image Anal*. 2008; 12:26–41. [PubMed: 17659998]
- Avants BB, et al. The Insight ToolKit image registration framework. *Front Neuroinform*. 2014; 8:44. [PubMed: 24817849]
- Badea A, et al. Quantitative mouse brain phenotyping based on single and multispectral MR protocols. *NeuroImage*. 2012; 63:1633–1645. [PubMed: 22836174]
- Badea A, et al. Remote sites of structural atrophy predict later amyloid formation in a mouse model of Alzheimer's disease. *NeuroImage*. 2010; 50:416–427. [PubMed: 20035883]
- Balint B, Bhatia KP. Isolated and combined dystonia syndromes – an update on new genes and their phenotypes. *European Journal of Neurology*. 2015; 22:610–617. [PubMed: 25643588]
- Bressman SB, et al. Idiopathic dystonia among ashkenazi jews: Evidence for autosomal dominant inheritance. *Annals of Neurology*. 1989; 26:612–620. [PubMed: 2817837]
- Calakos N, et al. Functional evidence implicating a novel TOR1A mutation in idiopathic, late-onset focal dystonia. *J Med Genet*. 2010; 47:646–650. [PubMed: 19955557]
- Calderon DP, et al. The neural substrates of rapid-onset Dystonia-Parkinsonism. *Nat Neurosci*. 2011; 14:357–365. [PubMed: 21297628]
- Carbon M, Eidelberg D. Abnormal structure-function relationships in hereditary dystonia. *Neuroscience*. 2009; 164:220–229. [PubMed: 19162138]
- Carbon M, et al. Microstructural white matter changes in carriers of the DYT1 gene mutation. *Annals of Neurology*. 2004a; 56:283–286. [PubMed: 15293281]
- Carbon M, et al. Microstructural white matter changes in primary torsion dystonia. *Movement Disorders*. 2008; 23:234–239. [PubMed: 17999428]
- Carbon M, et al. Regional metabolism in primary torsion dystonia: Effects of penetrance and genotype. *Neurology*. 2004b; 62:1384–1390. [PubMed: 15111678]
- Chen M, et al. Sapap3 deletion anomalously activates short-term endocannabinoid-mediated synaptic plasticity. *The Journal of Neuroscience*. 2011; 31:9563–9573. [PubMed: 21715621]
- Choi S, Lovinger DM. Decreased probability of neurotransmitter release underlies striatal long-term depression and postnatal development of corticostriatal synapses. *Proceedings of the National Academy of Sciences of the United States of America*. 1997; 94:2665–2670. [PubMed: 9122253]
- Chung HJ, et al. Phosphorylation of the AMPA Receptor Subunit GluR2 Differentially Regulates Its Interaction with PDZ Domain-Containing Proteins. *The Journal of Neuroscience*. 2000; 20:7258–7267. [PubMed: 11007883]
- Chung MK, et al. General multivariate linear modeling of surface shapes using SurfStat. *Neuroimage*. 2010; 53:491–505. [PubMed: 20620211]
- Dang MT, et al. An anticholinergic reverses motor control and corticostriatal LTD deficits in DYT1 GAG knock-in mice. *Behavioural Brain Research*. 2012; 226:465–472. [PubMed: 21995941]

- Dang MT, et al. Generation and characterization of DYT1 [Delta]GAG knock-in mouse as a model for early-onset dystonia. *Experimental Neurology*. 2005; 196:452–463. [PubMed: 16242683]
- Dauer WT, et al. Current concepts on the clinical features, aetiology and management of idiopathic cervical dystonia. *Brain*. 1998; 121:547–560. [PubMed: 9577384]
- de Carvalho Aguiar P, et al. Mutations in the Na<sup>+</sup>/K<sup>+</sup>-ATPase  $\alpha$ 3 Gene ATP1A3 Are Associated with Rapid-Onset Dystonia Parkinsonism. *Neuron*. 2004; 43:169–175. [PubMed: 15260953]
- DeAndrade MP, et al. Characterization of Atp1a3 mutant mice as a model of rapid-onset dystonia with parkinsonism. *Behavioural brain research*. 2011; 216:659–665. [PubMed: 20850480]
- Dobri i V, et al. Phenotype of non-c.907\_909delGAG mutations in TOR1A: DYT1 dystonia revisited. *Parkinsonism & Related Disorders*. 2015; 21:1256–1259. [PubMed: 26297380]
- Dufke C, et al. Screening of mutations in GNAL in sporadic dystonia patients. *Movement Disorders*. 2014; 29:1193–1196. [PubMed: 24408567]
- Eidelberg D, et al. Functional brain networks in DYT1 dystonia. *Annals of Neurology*. 1998; 44:303–312. [PubMed: 9749595]
- Ghilardi M-F, et al. Impaired sequence learning in carriers of the DYT1 dystonia mutation. *Annals of Neurology*. 2003; 54:102–109. [PubMed: 12838525]
- Gong S, et al. A gene expression atlas of the central nervous system based on bacterial artificial chromosomes. *Nature*. 2003; 425:917–925. [PubMed: 14586460]
- Goodchild RE, et al. Loss of the Dystonia-Associated Protein TorsinA Selectively Disrupts the Neuronal Nuclear Envelope. *Neuron*. 2005; 48:923–932. [PubMed: 16364897]
- Groen JL, et al. CACNA1B mutation is linked to unique myoclonus-dystonia syndrome. *Human Molecular Genetics*. 2015; 24:987–993. [PubMed: 25296916]
- Groen JL, et al. DRD1 rare variants associated with tardive-like dystonia: A pilot pathway sequencing study in dystonia. *Parkinsonism & Related Disorders*. 2014; 20:782–785. [PubMed: 24768614]
- Grundmann K, et al. Overexpression of human wildtype torsinA and human DeltaGAG torsinA in a transgenic mouse model causes phenotypic abnormalities. *Neurobiology of Disease*. 2007; 27:190–206. [PubMed: 17601741]
- Hettich J, et al. Biochemical and Cellular Analysis of Human Variants of the DYT1 Dystonia Protein, TorsinA/TOR1A. *Human Mutation*. 2014; 35:1101–1113. [PubMed: 24930953]
- Hewett JW, et al. Dystonia-causing mutant torsinA inhibits cell adhesion and neurite extension through interference with cytoskeletal dynamics. *Neurobiology of Disease*. 2006; 22:98–111. [PubMed: 16361107]
- Jew CP, et al. mGluR5 Ablation in Cortical Glutamatergic Neurons Increases Novelty-Induced Locomotion. *PLoS ONE*. 2013; 8:e70415. [PubMed: 23940572]
- Johnson GA, et al. Waxholm Space: An image-based reference for coordinating mouse brain research. *NeuroImage*. 2010; 53:365–372. [PubMed: 20600960]
- Johnson GA, et al. Morphologic Phenotyping with MR Microscopy: The Visible Mouse. *Radiology*. 2002; 222:789–793. [PubMed: 11867802]
- Kawashita E, et al. Altered Behavior in Mice with Deletion of the Alpha2-Antiplasmin Gene. *PLoS ONE*. 2014; 9:e97947. [PubMed: 24874880]
- Kock N, et al. Effects of genetic variations in the dystonia protein torsinA: identification of polymorphism at residue 216 as protein modifier. *Human Molecular Genetics*. 2006; 15:1355–1364. [PubMed: 16537570]
- Kumar KR, et al. Mutations in gnal: A novel cause of craniocervical dystonia. *JAMA Neurology*. 2014; 71:490–494. [PubMed: 24535567]
- Liang CC, et al. TorsinA hypofunction causes abnormal twisting movements and sensorimotor circuit neurodegeneration. *The Journal of Clinical Investigation*. 2014; 124:3080–3092. [PubMed: 24937429]
- Lohmann K, et al. Identification and functional analysis of novel THAP1 mutations. *European Journal of Human Genetics*. 2012; 20:171–175. [PubMed: 21847143]
- Martella G, et al. Regional specificity of synaptic plasticity deficits in a knock-in mouse model of DYT1 dystonia. *Neurobiology of Disease*. 2014; 65:124–132. [PubMed: 24503369]

- Martella G, et al. Impairment of bidirectional synaptic plasticity in the striatum of a mouse model of DYT1 dystonia: role of endogenous acetylcholine. *Brain*. 2009; 132:2336–2349. [PubMed: 19641103]
- Neychev VK, et al. The Functional Neuroanatomy of Dystonia. *Neurobiology of disease*. 2011; 42:185–201. [PubMed: 21303695]
- Nibbeling E, et al. Accumulation of rare variants in the arylsulfatase G (ARSG) gene in task-specific dystonia. *Journal of Neurology*. 2015; 262:1340–1343. [PubMed: 25825126]
- Niimi K, et al. Analysis of motor function and dopamine systems of SAMP6 mouse. *Physiology & Behavior*. 2009; 96:464–469. [PubMed: 19084029]
- Nutt JG, et al. Epidemiology of focal and generalized dystonia in Rochester, Minnesota. *Movement Disorders*. 1988; 3:188–194. [PubMed: 3264051]
- Oleas J, et al. Rodent Models of Autosomal Dominant Primary Dystonia. *Movement Disorders: Genetics and Models: Second Edition*. 2014:483–505.
- Ozelius L, L N. DYT1 Early-Onset Primary Dystonia. *GeneReviews® [Internet]*. 1999 [Updated 2014].
- Ozelius LJ, et al. The early-onset torsion dystonia gene (DYT1) encodes an ATP-binding protein. *Nat Genet*. 1997; 17:40–48. [PubMed: 9288096]
- Pappas SS, et al. Forebrain deletion of the dystonia protein torsinA causes dystonic-like movements and loss of striatal cholinergic neurons. *eLife*. 2015; 4:e08352. [PubMed: 26052670]
- Risch NJ, et al. Segregation analysis of idiopathic torsion dystonia in Ashkenazi Jews suggests autosomal dominant inheritance. *American Journal of Human Genetics*. 1990; 46:6.
- Saunders-Pullman R, et al. Heterogeneity in primary dystonia: Lessons from THAP1, GNAL, and TOR1A in Amish-Mennonites. *Movement Disorders*. 2014; 29:812–818. [PubMed: 24500857]
- Shuen JA, et al. Drd1a-tdTomato BAC Transgenic Mice for Simultaneous Visualization of Medium Spiny Neurons in the Direct and Indirect Pathways of the Basal Ganglia. *The Journal of Neuroscience*. 2008; 28:2681–2685. [PubMed: 18337395]
- Song CH, et al. Subtle microstructural changes of the cerebellum in a knock-in mouse model of DYT1 dystonia. *Neurobiol Dis*. 2014; 62:372–380. [PubMed: 24121114]
- Tanabe LM, et al. Primary dystonia: molecules and mechanisms. *Nature reviews. Neurology*. 2009; 5:598–609. [PubMed: 19826400]
- Tanabe LM, et al. Genetic background modulates the phenotype of a mouse model of DYT1 dystonia. *PLoS One*. 2012; 7:e32245. [PubMed: 22393392]
- Trošt M, et al. Primary dystonia: Is abnormal functional brain architecture linked to genotype? *Annals of Neurology*. 2002; 52:853–856. [PubMed: 12447944]
- Ulug AM, et al. Cerebellothalamocortical pathway abnormalities in torsinA DYT1 knock-in mice. *Proceedings of the National Academy of Sciences of the United States of America*. 2011; 108:6638–6643. [PubMed: 21464304]
- Vasudevan A, et al. Developmental patterns of torsinA and torsinB expression. *Brain Research*. 2006:1073–1074. 139–145.
- Vemula SR, et al. A rare sequence variant in intron 1 of THAP1 is associated with primary dystonia. *Molecular Genetics & Genomic Medicine*. 2014; 2:261–272. [PubMed: 24936516]
- Vo A, et al. Early registration of diffusion tensor images for group tractography of dystonia patients. *Journal of Magnetic Resonance Imaging*. 2013a; 37:67–75. [PubMed: 22987473]
- Vo A, et al. White matter changes in primary dystonia determined by 2D distribution analysis of diffusion tensor images. *J Magn Reson Imaging*. 2013b; 37:59–66. [PubMed: 22987399]
- Vo A, et al. FDG-microPET and MR DTI findings in Tor1a heterozygous knock-out mice. *Neurobiology of Disease*. 2014; 73c:399–406. [PubMed: 25447231]
- Vulinovic F, et al. Unraveling Cellular Phenotypes of Novel TorsinA/TOR1A Mutations. *Human Mutation*. 2014; 35:1114–1122. [PubMed: 24931141]
- Wan Y, et al. Sapap3 deletion causes mGluR5-dependent silencing of AMPAR synapses. *The Journal of Neuroscience*. 2011; 31:16685–16691. [PubMed: 22090495]
- Zech M, et al. Rare sequence variants in ANO3 and GNAL in a primary torsion dystonia series and controls. *Movement Disorders*. 2014; 29:143–147. [PubMed: 24151159]

- Ziegan J, et al. Novel GNAL mutations in two German patients with sporadic dystonia. *Movement Disorders*. 2014; 29:1833–1834. [PubMed: 25382112]
- Zweig RM, et al. Pathology in brainstem regions of individuals with primary dystonia. *Neurology*. 1988; 38:702–706. [PubMed: 3362365]

Author Manuscript

Author Manuscript

Author Manuscript

Author Manuscript

### Highlights

- A rare TOR1A variant reduces steady-state TorsinA levels in humans and mice
- Mice homozygous for the rare variant show motor abnormalities
- Mutant mice also show altered striatal synaptic plasticity and brain neuroimaging
- These results connect TorsinA dysfunction to rare presentations of sporadic disease
- F205I/F205I mutant mice provide a new model to examine dystonia pathogenesis

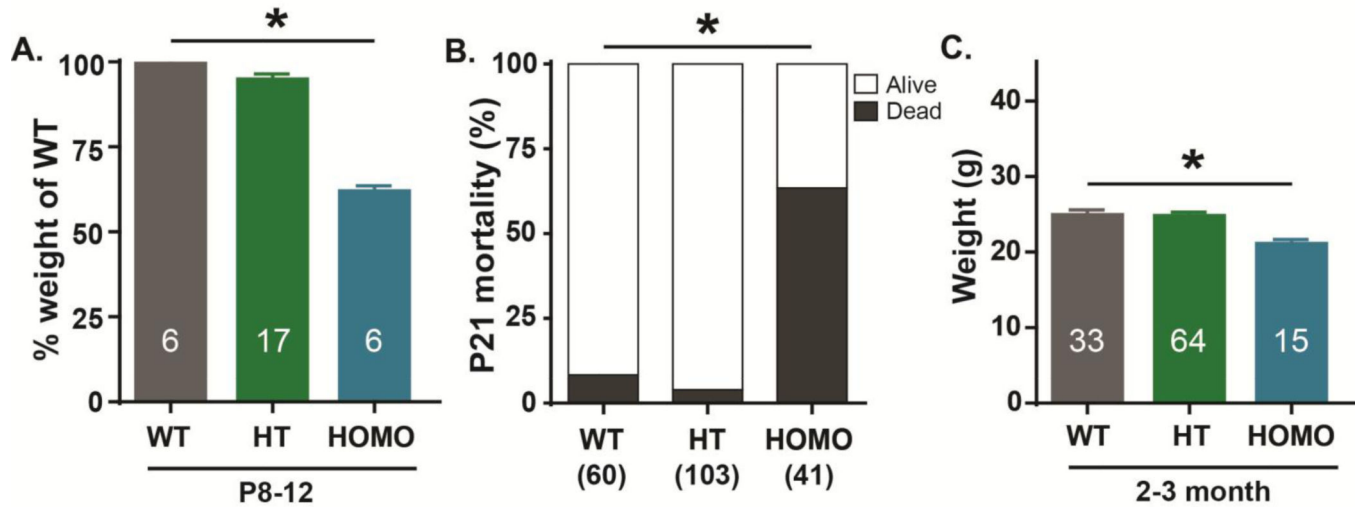


**Figure 1. F205I homozygotes have increased mortality and weigh less than WT**

(A) F205I homozygous, but not heterozygous, mice have marked weight loss in the second week of life, compared to wildtype mice (HT  $94.75 \pm 1.72\%$  of WT, HOMO  $61.79 \pm 1.74\%$  of WT; WT vs HOMO  $p < 0.0001$ , WT vs HT  $p > 0.05$ , one-way ANOVA, Dunnett's *post hoc*;  $n = 6$  WT, 17 HT, 6 HOMO). (B) F205I homozygotes, but not heterozygotes, had significantly increased mortality in the first 3 weeks of life compared to wildtype mice (WT 8.33%, HT 3.96%, HOMO 63.41%; WT vs HOMO  $p < 0.0001$ , WT vs HT  $p > 0.05$ , Chi-square;  $n = 60$  WT, 103 HT, 41 HOMO). (C) By 2 to 3 months of age, homozygous mice regain weight to near normal levels, though they still weigh significantly less than wildtype mice (WT  $24.85 \pm 0.76$  g, HT  $24.74 \pm 0.56$  g, HOMO  $21.01 \pm 0.65$  g; WT vs HOMO  $p < 0.01$ , WT vs HT  $p > 0.05$ , one-way ANOVA, Dunnett's *post hoc*;  $n = 33$  WT, 64 HT, 15 HOMO).

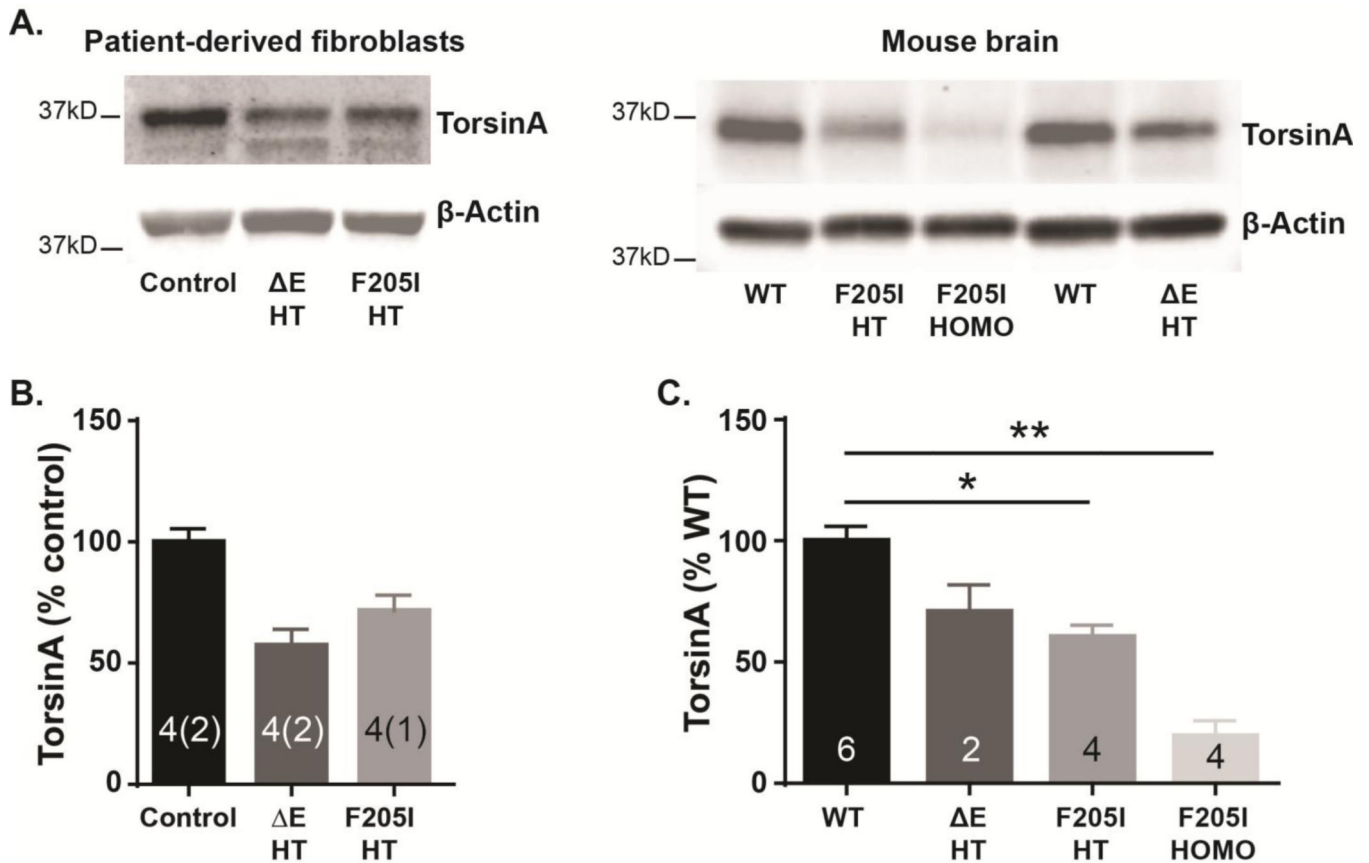


**Figure 2. TorsinA protein levels are reduced in F205I human fibroblasts and mouse brain**  
**(A)** Representative Western blots for TorsinA (37 kD) in patient-derived fibroblast cell lines and mouse whole cortical extracts.  $\beta$ -actin (42 kD) was used as a loading control. **(B)** Quantification of Westerns shows TorsinA is reduced in fibroblasts of  $\Delta E$  ( $57.36 \pm 6.59$  % of WT) and F205I patients ( $71.72 \pm 6.29$  % of WT;  $n = 4$  independent experimental replicates from the F205I line (a single patient) and 2 replicates for each of 2 healthy control cell lines and 2 cell lines derived from  $\Delta E$  DYT1-affected individuals. Error bars and statistics are based on experimental replicates ( $n = 4$ ) due to availability of only a single patient with F205I. **(C)** Quantification of Westerns shows TorsinA levels are reduced in mouse models of TorsinA mutations. Whole cortical extracts of F205I heterozygote mice have significantly less TorsinA than wildtype littermates ( $60.42 \pm 4.80$  % of WT;  $p < 0.05$ , one-way ANOVA, Holm-Sidak *post hoc*).  $\Delta E$  heterozygote mice show a similar reduction. F205I homozygote mice have significantly reduced TorsinA levels compared to both wildtype ( $19.56 \pm 6.28$  % of WT;  $p < 0.0001$ ) and F205I heterozygote mice ( $p < 0.05$ ; independent samples prepared from 6 WT mice, 4 F205I HT mice, 4 F205I HOMO mice, 2  $\Delta E$  HT mice).

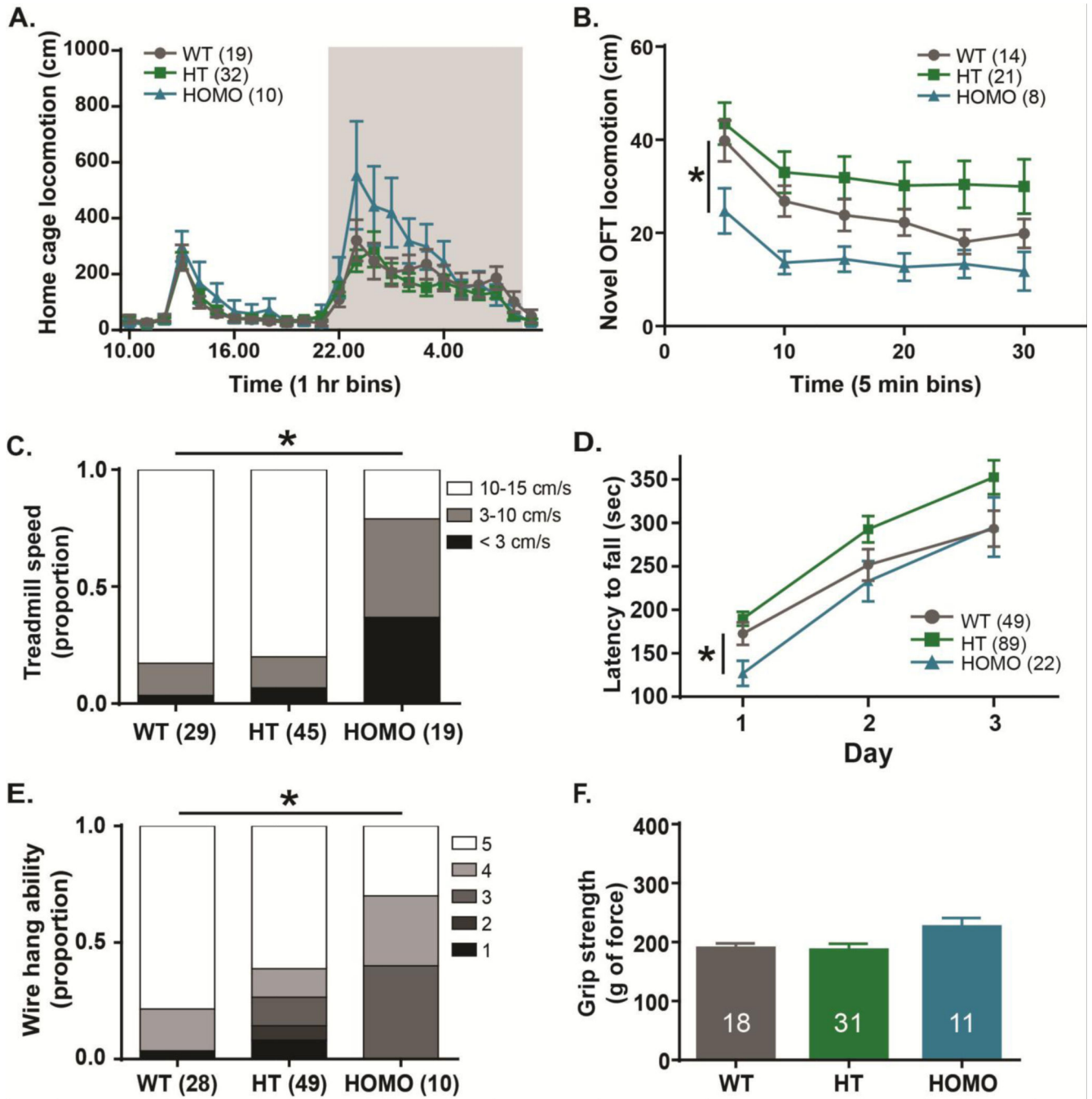


**Figure 3. F205I homozygotes have abnormal motor performance in novel environments**  
 (A) In a home-cage-like environment, locomotion of F205I homozygous and heterozygous mice was not significantly different from wildtype mice throughout a full 24-hour cycle ( $p > 0.05$ , two-way ANOVA;  $n = 19$  WT, 32 HT, 10 HOMO). Shaded area indicates the dark cycle. (B) In a novel environment, homozygous mice had lower activity ( $p < 0.05$ , genotype effect, two-way ANOVA; WT vs HOMO  $p < 0.05$ , WT vs HT  $p > 0.05$ , Holm-Sidak *post hoc*;  $n = 14$  WT, 21 HT, 8 HOMO). (C) In the treadmill task, homozygous mice were unable to perform the task at typical walking speeds (WT vs HOMO  $p < 0.0001$ , Chi-square).

Heterozygous mice performed the task similarly to wildtype mice (WT vs HT  $p > 0.05$ , Chi-square;  $n = 29$  WT, 45 HT, 19 HOMO). **(D)** In the 3-day accelerating rotarod task, homozygous mice performed worse than wildtype mice on the first day of testing (WT  $172.5 \pm 12.7$  seconds, HOMO  $127.0 \pm 14.6$  seconds;  $p < 0.05$ , one-way ANOVA, Dunnett's *post hoc*). Heterozygous mice performed similarly to wildtype mice on all days ( $p > 0.05$ , one-way ANOVA, Dunnett's *post hoc*). With repeated days of testing, homozygous mice performed similarly to wildtype mice ( $p > 0.05$ , one-way ANOVA), indicating intact motor learning. There was no significant difference in the rate of improvement ( $p > 0.05$  genotype $\times$ time, two-way ANOVA;  $n = 49$  WT, 89 HT, 22 HOMO). **(E)** Wire hang motor coordination was impaired in F205I homozygotes, but not heterozygotes (WT vs. HOMO  $p < 0.05$ , WT vs. HT  $p > 0.05$ , Fisher's exact test;  $n = 28$  WT, 49 HT, 10 HOMO). **(F)** Grip strength was similar across all genotypes (WT  $202.2 \pm 17.62$  g of force, HT  $168.6 \pm 10.49$  g of force, HOMO  $230.3 \pm 28.96$  g of force;  $p > 0.05$ , one-way ANOVA;  $n = 18$  WT, 31 HT, 11 HOMO).

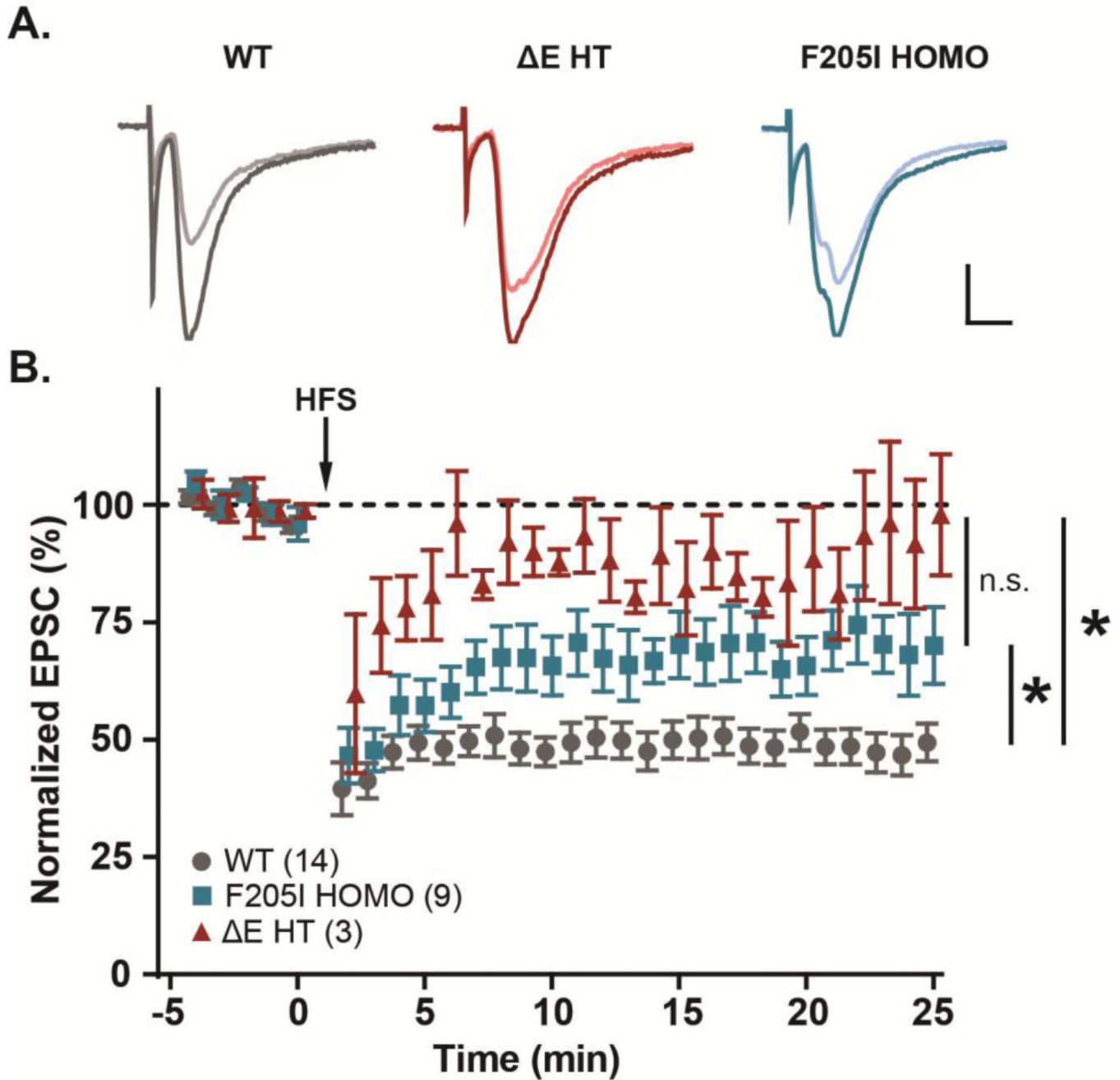


**Figure 4. Corticostriatal long-term depression (LTD) is reduced in F205I homozygote mice**  
Corticostriatal LTD was induced by high frequency stimulation (HFS, 4 trains, 100 Hz, paired with 0 mV post-synaptic depolarization). EPSC amplitudes were normalized to the pre-HFS baseline. **(A)** Representative traces showing LTD observed (lighter traces) for each genotype, normalized to baseline EPSC (darker traces). Scale bar indicates 25% of baseline response (y-axis) and 5 ms (x-axis). **(B)** F205I homozygotes and  $\Delta E$  heterozygotes had reduced LTD magnitude compared to WT mice. WT littermate controls for each line ( $\Delta E$  and F205I) were no different and were combined. (WT  $49.05 \pm 3.96\%$ , F205I HOMO  $70.03$

$\pm 9.03\%$ , E HT  $97.90 \pm 12.90\%$ ; n = WT 14 cells, 5 mice; F205I HOMO 9 cells, 3 mice; E HT, 3 cells, 2 mice; WT vs F205I  $p < 0.05$ , WT vs E  $p < 0.05$ , F205I vs E  $p > 0.05$ , one-way ANOVA, Holm-Sidak *post hoc*).

Author Manuscript

Author Manuscript

Author Manuscript

Author Manuscript

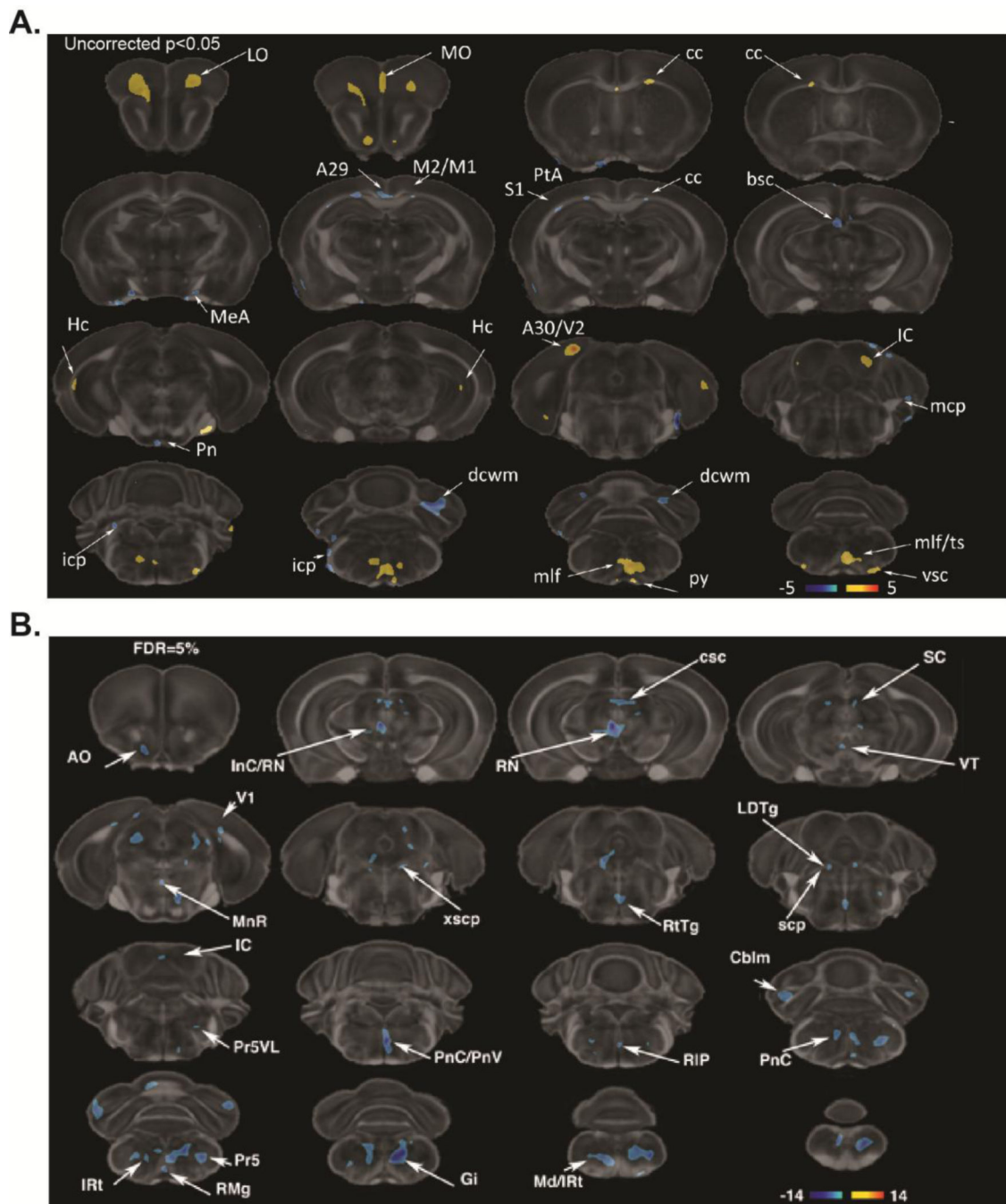


**Figure 5. F205I homozygotes have fractional anisotropy (FA) and volume changes on MRI**  
**(A)** Changes in FA occurred both as decreases and increases in F205I mice, indicating reductions in some white matter tracts and enhancement of other white matter tracts. FA was increased in areas of corpus callosum (cc); pontine structures (py, vsc); medial lemniscus (ml); medial longitudinal fasciculus (mlf, mlf/ts); hippocampus (Hc); border of visual cortex near corpus callosum (A30/V2); inferior colliculus (IC); and medial and lateral orbital cortices (MO, LO). FA was decreased for corpus callosum in the areas below the cingulate cortex (A29), motor cortices (M1/M2), parietal association cortex (PtA) and S1; deep

cerebellar white matter (dcwm); brachium of superior colliculus (bsc); inferior cerebellar peduncles (icp); and medial amygdaloid nucleus (MeA) (uncorrected  $p < 0.05$ ;  $n = 6$  WT, 5 HOMO mice). Some clusters were not symmetric in the same coronal slices; however, a contralateral cluster was found in neighboring slices. **(B)** Voxel-based morphometry of volume changes showed F205I homozygotes had lower brain volume in anterior olfactory nuclei (AO); interstitial nucleus of Cajal (InC); red nucleus (RN); superior colliculus (SC); tegmentum (RtTg, LDTg); median raphe nuclei (MnR); inferior colliculus (IC); pons (PnC, Gi, RIP); reticular medullary nuclei (IRt, RMg); Pr5 (Pr5, Pr5VL); cerebellum (Cblm); commissure of the superior colliculus (csc); and the decussation of the superior cerebellar peduncles (xcsp) (5% FDR corrected  $p < 0.05$ ;  $n = 6$  WT, 6 HOMO mice). Images are rostral to caudal, coronal views.